Available online at www.sciencedirect.com
ScienceDirect
Polymer 48 (2007) 2425–2433
polymer
www.elsevier.com/locate/polymer

Surface morphology evolution of poly(styrene-*block*-4-vinylpyridine) (PS-*b*-P4VP)(H^+) and poly(methyl methacrylate)-dibenzo-18-crown-6-poly(methyl methacrylate) (PMCMA) supramolecular film

Junpeng Gao [a], Ping Zhang [a], Jun Fu [a], Binyao Li [a], Yanchun Han [a,*], Xiang Yu [b], Caiyuan Pan [b]

[a] *State Key Laboratory of Polymer Physics and Chemistry, Changchun Institute of Applied Chemistry, Chinese Academy of Sciences, Graduate School of the Chinese Academy of Sciences, 5625 Renmin Street, Changchun, Jilin 130022, PR China*
[b] *Department of Polymer Science and Engineering, University of Science and Technology of China, Hefei 230026, PR China*

Received 22 August 2006; received in revised form 11 January 2007; accepted 7 February 2007
Available online 15 February 2007

Abstract

Well-ordered nanostructured polymeric supramolecular thin films were fabricated from the supramolecular assembly of poly(styrene-*block*-4-vinylpyridine) (PS-*b*-P4VP)(H^+) and poly(methyl methacrylate)-dibenzo-18-crown-6-poly(methyl methacrylate) (PMCMA). A depression of cylindrical nanodomains was formed by the block of P4VP(H^+) and PMCMA associates surrounded by PS. The repulsive force aroused from the incompatibility between the block of P4VP(H^+) and PMCMA was varied through changing the molecule weight (M_w) of PMCMA, the volume fraction of the block of P4VP(H^+), and annealing the film at high temperature. Increasing the repulsive force led to a change of overall morphology from ordered nanoporous to featureless structures. The effects of solvent nature and evaporation rate on the film morphology were also investigated. Further evolution of surface morphologies from nanoporous to featureless to nanoporous structures was observed upon exposure to carbon bisulfide vapors for different treatment periods. The wettability of the film surface was changed from hydrophilicity to hydrophobicity due to the changes of the film surface microscopic composition.

Keywords: Nanostructure; Self-assembly; Electrostatic interaction

1. Introduction

During the past decade, many research activities have been done in preparation of the nanometer-sized structures stimulated by the continuing demand for miniaturization of devices and electronic components [1,2]. Due to the limitation of conventional lithographic techniques, fabrication of nanostructures less than 100 nm is difficult. So there is an obvious need for alternative ‘‘bottom-up’’ approaches. The use of self-assembly to prepare well-ordered structures has attracted increasing interest due to the ease of accessing complex structures with small feature sizes [3–10]. Because of the connectivity constraints and incompatibility between the two blocks, diblock copolymer spontaneously self-assembles into micro-separated nanometer-sized domains that exhibit ordered morphologies at equilibrium [11]. The microdomain structure in block copolymer thin film has been investigated extensively in experiments [2,12–21], theory [22–24], and simulation [25–29]. In recent years, self-organized nanostructures of polymeric supramolecules offer an efficient pathway to construct ordered nanostructures and functional materials on the basis of physical interactions, such as ionic interactions [30], coordination bond [31–37], and hydrogen bond [38–43,46] between the repulsive blocks, allowing also the hierarchical order and functional materials [1,44,45]. For example, Ikkala and coworkers demonstrated that amphiphilic molecules could be hydrogen bonded to the pyridine groups of PS-*b*-P4VP, allowing structural hierarchy, and mesoporous materials with

* Corresponding author. Tel.: +86 431 85262175; fax: +86 431 85262126.
E-mail address: ychan@ciac.jl.cn (Y. Han).

0032-3861/$ - see front matter © 2007 Elsevier Ltd. All rights reserved.
doi:10.1016/j.polymer.2007.02.025

cylindrical pores were obtained after selective removal of the amphiphiles [38,40,44,47]. Organized molecular films, fabricated mainly by the Langmuir–Blodgett method and self-assembling techniques can also be prepared based on hydrogen bonding and have been progressed greatly [48,49]. The introduction of metal coordination into the main chain of a polymer leads to reversible supramolecular materials [50]. Upon addition of a competing ligand, a reversible opening of the metal complex could be achieved, opening a pathway toward new ''switchable'' functional materials [51]. The ionic interactions between polyelectrolytes and oppositely charged surfactants are quite strong and can induce complex formation, often resulting in highly ordered structures [52–55]. Both electrostatic interactions between the charged components and hydrophobic interactions between the polymer backbone and alkyl chains of the surfactant are important in driving the self-assembly of molecules to form ordered structures [52].

Herein, we report an alternative approach to prepare nanostructured films by self-assembly of a polymeric supramolecule, which consists of PS-*b*-P4VP(H^+) and PMCMA. The electrostatic interaction between the P4VP(H^+) block and the crown ether moieties in PMCMA is utilized to drive the formation of supramolecules. Combining the electrostatic interaction and the solubility of polymers in a certain solvent, a depression of cylindrical nanodomains can be formed by the block of P4VP(H^+) and PMCMA associates surrounded by PS. The effects of solvent nature and evaporation rate on the film morphology are investigated. Through increasing the molecular weights of PMCMA and P4VP blocks and annealing the nanoporous film at high temperatures, the repulsive force between PMCMA and P4VP(H^+) is increased. A change of overall morphology from ordered nanoporous to featureless structure is observed. On exposure of a certain film to a solvent selective for PS at room temperature for different times, different morphologies and surface properties can be obtained. The possible formation mechanisms of the nanostructures in the polymeric supramolecular films are discussed in detail.

2. Experimental part

2.1. Materials

The diblock copolymers PS-*b*-P4VP ($M_{w,\,PS} = 31\,900$ g/mol, $M_{w,\,P4VP} = 13\,200$ g/mol, $M_w/M_n = 1.08$) and PS-*b*-P4VP ($M_{w,\,PS} = 21\,400$ g/mol, $M_{w,\,P4VP} = 20\,700$ g/mol, $M_w/M_n = 1.13$) were obtained from Polymer Source, Inc. The designed two-armed polymers with crown ether core, poly(methyl methacrylate)-dibenzo-18-crown-6-poly(methyl methacrylate) (PMCMA) ($M_w = 7200$, $M_w/M_n = 1.18$; $M_w = 36\,700$, $M_w/M_n = 1.25$) (Scheme 1) were synthesized by atom transfer radical polymerization (ATRP) [56]. Chloroform (A.R. grade), carbon bisulfide and tetrahydrofuran (A.R. grade) (THF) were supplied by Beijing Chemical Reagent Company. Deionized (DI) water was obtained using the millipore water purification system. All glasswares were washed with aqua regia solution (H_2SO_4/K_2CrO_4) under sonication for 10 min in an ultrasonic bath and rinsed thoroughly with DI water. The silicon substrates

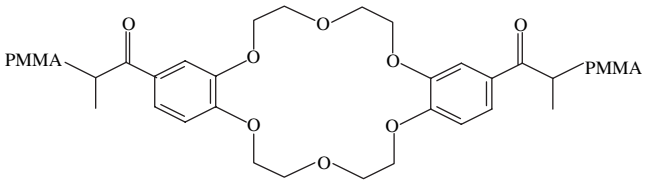

Scheme 1. Chemical structure of the two-armed polymer with crown ether core, poly(methyl methacrylate)-dibenzo-18-crown-6-poly(methyl methacrylate) (PMCMA).

with about 2 nm thick layer of native SiO_x were cleaned by immersion in piranha solution (3:1 concentrated H_2SO_4/30% H_2O_2) and sonication for 30 min. Subsequently, the substrates were rinsed repeatedly with DI water and blown dry in an N_2 flow.

2.2. Sample preparation

The diblock copolymers, PS-*b*-P4VP and PMCMA were dissolved in chloroform or tetrahydrofuran with a certain concentration. The pH value in solutions was adjusted to about 3 using 4 M hydrochloric acid to protonate the pyridine units. The solutions were stirred for 3 days before being spin-coated (~2000 rpm) or cast onto the pre-cleaned silicon wafers. Without removing the residual solvent, the samples were exposed to saturated carbon bisulfide vapor in a closed vessel and kept at room temperature for various periods (5–93 h). Some solutions were cast onto the copper mesh grids to fabricate the sample for transmission electron microscopic (TEM) characterization. Staining was achieved by treating the film for 10 h with RuO_4 vapor. All the films were finally dried at room temperature in a vacuum for 48 h to remove any residual solvent. Two films were fabricated by spin-coating the solution containing PS(31 900)-*b*-P4VP(13 200)(H^+) and PMCMA(7200) onto silicon wafers. One film was annealed at 112 °C for 24 h without removing the residual solvents, and the other film was annealed at 160 °C for 12 h after removing the residual solvents.

2.3. Instruments

Atomic force microscopy (AFM) was performed on a commercial scanning probe microscopy (SPA 300HV with an SPI 3800N probe station, Seiko Instruments Inc., Japan) in tapping mode. A silicon microcantilever (spring constant 2 N/m^{-1} and resonance frequency 70 kHz, Olympus, Japan) with an etched conical tip (radius of curvature 40 nm as characterized by scanning over very sharp needle array, NT-MDT, Russia) was used for scan. Water contact angles were determined using a KRÜSS DSA10-MK2 contact angle measuring system at room temperature. The probe fluid used was DI water and the drop volume was 2 μL. Fourier transform infrared spectra (FTIR) were recorded with a Bruker Vertex 70 FT-IR spectrometer equipped with a DTGS detector (scan numbers: 32, resolution: 4 cm^{-1}). Samples were prepared by solvent casting from chloroform onto potassium bromide crystal.

X-ray photoelectron spectra (XPS) were measured with VG ESCALAB MK (VG Company, UK) at room temperature by using an Mg Kα X-ray source ($hv = 1253.6$ eV) at 14 kV and 20 mA. The sample analysis chamber of the XPS instrument was maintained at a pressure of 1×10^{-7} Pa. TEM study was performed on a JEM-1011 transmission electron microscopy (JEOL Inc., Japan) operated at 100 kV accelerating voltage. Small-Angle X-ray Scattering (SAXS) was performed on an evacuated Kratky compact camera (Kratky PW1700 X-ray scatteractometer, Holland). The X-ray source is a sealed X-ray tube with copper anode working at 45 kV and 40 mA. The wavelength λ of Cu Kα is 0.154 nm. The primary data were plotted as the scattering intensity (I) vs the scattering vector, $q = 4\pi \sin\theta/\lambda$ (θ = scattering angle).

3. Results and discussion

In diblock copolymer PS-*b*-P4VP, pyridine is a strong base. When it is mixed with hydrochloric acid in solution, charge transfer from acid to a lone electron pair is expected to take place [57,58]. Therefore, the P4VP block can be positively charged after protonation. In the two-armed polymers used in this work, the crown ether with crown-like stereo (Scheme 2) exhibits electronegative property. The electrostatic interaction is expected to occur between P4VP(H^+) and crown ether when PS-*b*-P4VP(H^+) is mixed with PMCMA.

The film surface morphologies of PS(31 900)-*b*-P4VP(13 200) (1.00 wt%), PS(31 900)-*b*-P4VP(13 200)(H^+) (1.00 wt%), a mixture of PS(31 900)-*b*-P4VP(13 200) (1.00 wt%, without protonation) and PMCMA (0.29 wt%, $M_w = 7200$), PS(31 900)-*b*-P4VP(13 200)(H^+) (1.00 wt%) and PMCMA (0.29 wt%, $M_w = 7200$) are shown in Fig. 1 after spin-coating the solutions from a common solvent, chloroform. The film surface of PS(31 900)-*b*-P4VP(13 200) (film thickness: 234 nm) (Fig. 1(a)) was featureless and flat. A featureless film (film thickness: 236 nm) morphology was also obtained after spin-coating PS-*b*-P4VP(H^+) from chloroform (Fig. 1(b)). The possible reason may be that the electrostatic repulsive interaction among the P4VP(H^+) chains hindered the formation of ordered structures. For the film of PMCMA(7200) mixed with PS(31 900)-*b*-P4VP(13 200) (film thickness: 256 nm) (without protonation), macrophase separation was observed (Fig. 1(c)) because there are no attractive interactions but only the repulsive force between these two immiscible polymers exists. However, the electrostatic interaction may exist between the block of P4VP(H^+) and crown ether moieties in PMCMA. Meanwhile the electrostatic repulsive interaction among P4VP(H^+) chains might decrease due to the attractive interactions among the chains of PMCMA, which is joined with P4VP(H^+) by electrostatic interaction. To confirm the association between P4VP(H^+) and PMCMA, FTIR spectroscopy was used. The infrared spectra of (A) PS(31 900)-*b*-P4VP(13 200), (B) PS(31 900)-*b*-P4VP(13 200)(H^+) and (C) PS(31 900)-*b*-P4VP(13 200)(H^+)/PMCMA are shown in Fig. 2. A nitrogen–hydrogen stretching absorption band is observed at 3386 cm^{-1} after the protonation of pyridine, which is not observed in PS-*b*-P4VP. When PMCMA is added, the absorption band is shifted to 3406 cm^{-1} due to the association between P4VP(H^+) and PMCMA. So, the association is confirmed. It might be expected that the film has a lamellar structure in the equilibrium state after spin-coating the solution containing PS(31 900)-*b*-P4VP(13 200)(H^+) (1.00 wt%) and PMCMA (0.29 wt%, $M_w = 7200$) because the weight ratio between P4VP(H^+)/PMCMA and PS is 0.45/0.55. However, an array of nanoscopic cylindrical domains is seen at the surface of the film (film thickness: 256 nm), where the component of P4VP(H^+) and PMCMA forms the cylindrical domains (lighter in the phase image) and PS forms the matrix (darker in the phase image) (Fig. 1(d,e)), and the area occupied by P4VP(H^+)/PMCMA and PS is nearly consistent with the weight ratio between them. As we know, the film morphology is influenced by both thermodynamic and kinetic considerations under the conditions imposed by solvent casting. The morphology obtained by spin-coating is far from equilibrium morphology. So, controlled by kinetics, the final film morphology with cylindrical P4VP(H^+)/PMCMA nanodomains was formed in the nonequilibrium state due to the fast evaporation rate of chloroform. The cylindrical P4VP(H^+)/PMCMA nanodomains (the center to center interval of the cylinders is 47 nm) were depressed compared to the PS matrix and regular holes of about 5 nm in depth and 26 nm in diameter were formed. It is known that the polymer domains exhibiting higher solubility in the common solvent were observed to depress over the polymer domains with lower solubility [59]. The lower solubility phase solidifies first, while the higher solubility phase still contains some solvents and will therefore continue to shrink on complete solvent extraction, resulting in a depressed morphology [59,60]. Chloroform [$\delta_{chloroform} = 9.3$ (cal $cm^{-3})^{1/2}$] is a better solvent for PMCMA [$\delta_{PMCMA} = 9.3$ (cal $cm^{-3})^{1/2}$] and P4VP [$\delta_{P4VP} = 9.2$ (cal $cm^{-3})^{1/2}$] than for PS [$\delta_{PS} = 9.1$ (cal $cm^{-3})^{1/2}$] [59]. Therefore, it is reasonable that chloroform may lead to a depression of the P4VP(H^+) and PMCMA phases with respect to the PS phase [59]. Thus, the cylindrical P4VP(H^+) and PMCMA nanodomains were depressed compared to the PS matrix and left regular holes on the film surface.

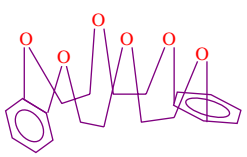

Scheme 2. The crown-like stereo of crown ether core.

The morphology obtained by spin-coating is far from equilibrium as mentioned above, and the degree of lateral order is low because of the rapid evaporation of solvent. To investigate the effect of solvent evaporation rate on the film surface morphology, a chloroform solution containing PS(31 900)-*b*-P4VP(13 200)(H^+) (1.00 wt%) and PMCMA (0.29 wt%, $M_w = 7200$) was cast onto the silicon substrate, and subsequently dried at ambient atmosphere. The temperature is about 20 °C and the relative humidity is around 25%. Holes were

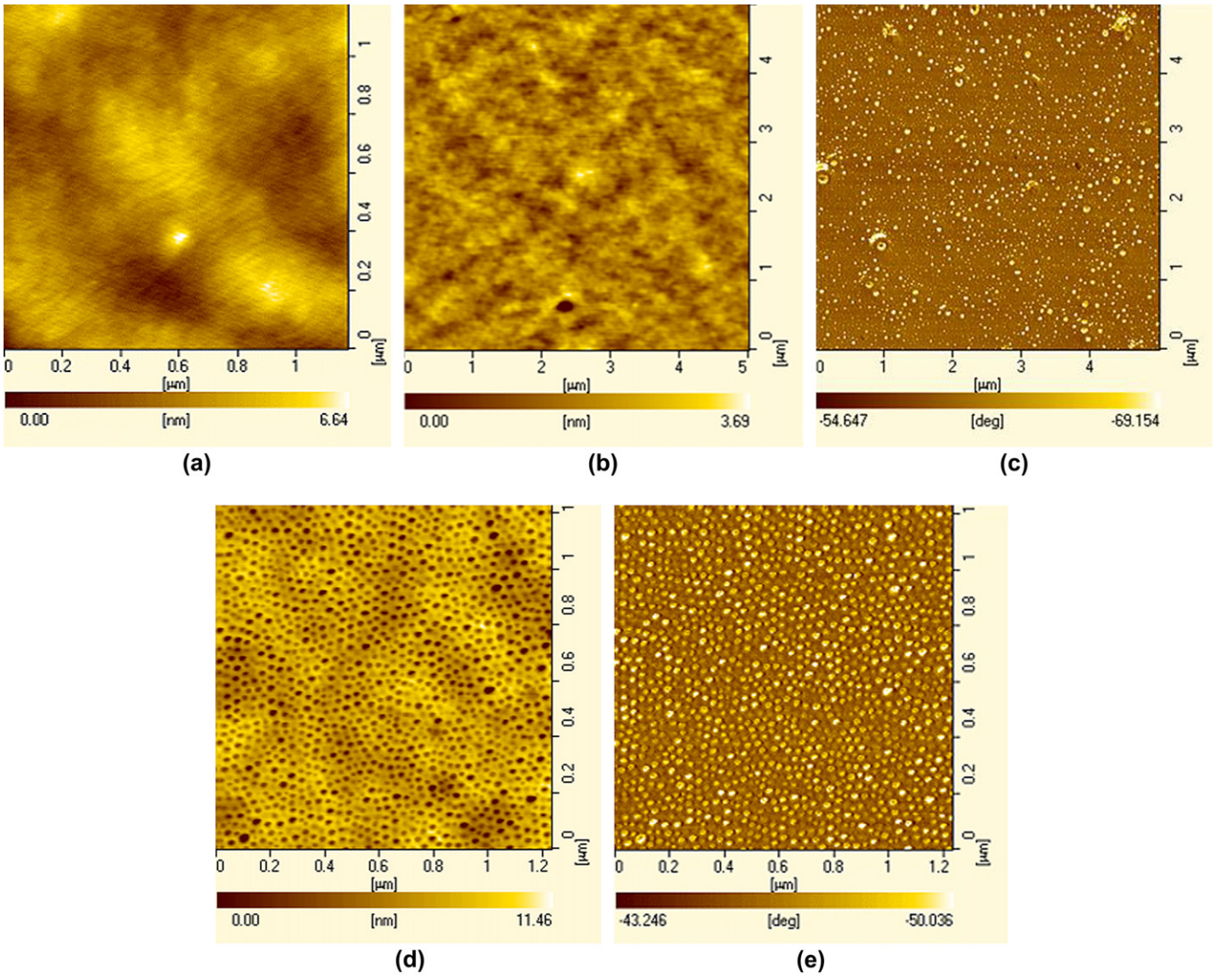

Fig. 1. AFM images of the thin film surface after spin-coating from the chloroform solution of (a) PS(31 900)-*b*-P4VP(13 200) (1.00 wt%), (b) PS(31 900)-*b*-P4VP(13 200)(H^+) (1.00 wt%), (c) the phase image of PS(31 900)-*b*-P4VP(13 200) (1 wt%, without protonation) and PMCMA (0.29 wt%, $M_w = 7200$), (d) topographic image and (e) phase image of PS(31 900)-*b*-P4VP(13 200)(H^+) (1.00 wt%) and PMCMA (0.29 wt%, $M_w = 7200$).

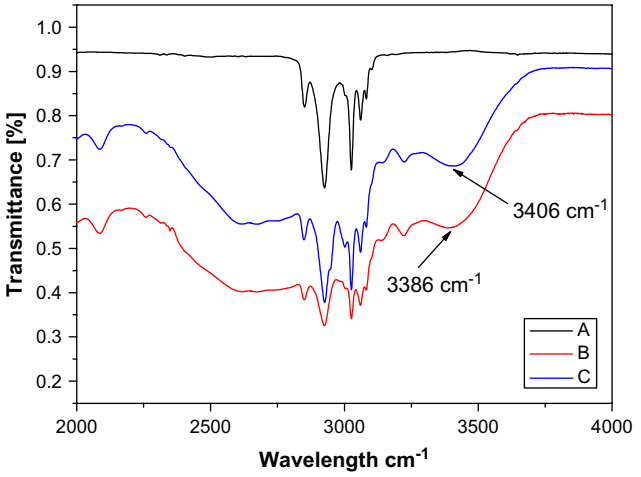

Fig. 2. FTIR spectra of (A) PS(31 900)-*b*-P4VP(13 200), (B) PS(31 900)-*b*-P4VP(13 200)(H^+) and (C) PS(31 900)-*b*-P4VP(13 200)(H^+)/PMCMA.

also found on the film surface, and the average size is about 10 nm and 26 nm in depth and diameter, respectively (Fig. 3(a)). Compared with the holes formed in the spin-coated film (Fig. 1(d)), the depth is larger but the diameter is the same. As we know, the speed of solvent evaporation during spin-coating is larger than that of free solvent evaporation. Under the condition of fast evaporation, kinetic arrest in the polymer might have taken place before the chains had enough time to make the rearrangements needed to obtain any equilibrium morphology occurred in the course of the evaporation [61]. This is analogous to fast quenching of a disordered block copolymer melt from elevated temperatures. Therefore, the P4VP(H^+) and PMCMA microdomains could solidify first during the process of spin-coating while the microdomains would still be able to shrink in the films under low evaporation rate. Thus, the holes formed under low evaporation rate are more ordered than those during the process of spin-coating approach equilibrium (Figs. 1(e) and 3(b)). However, even under

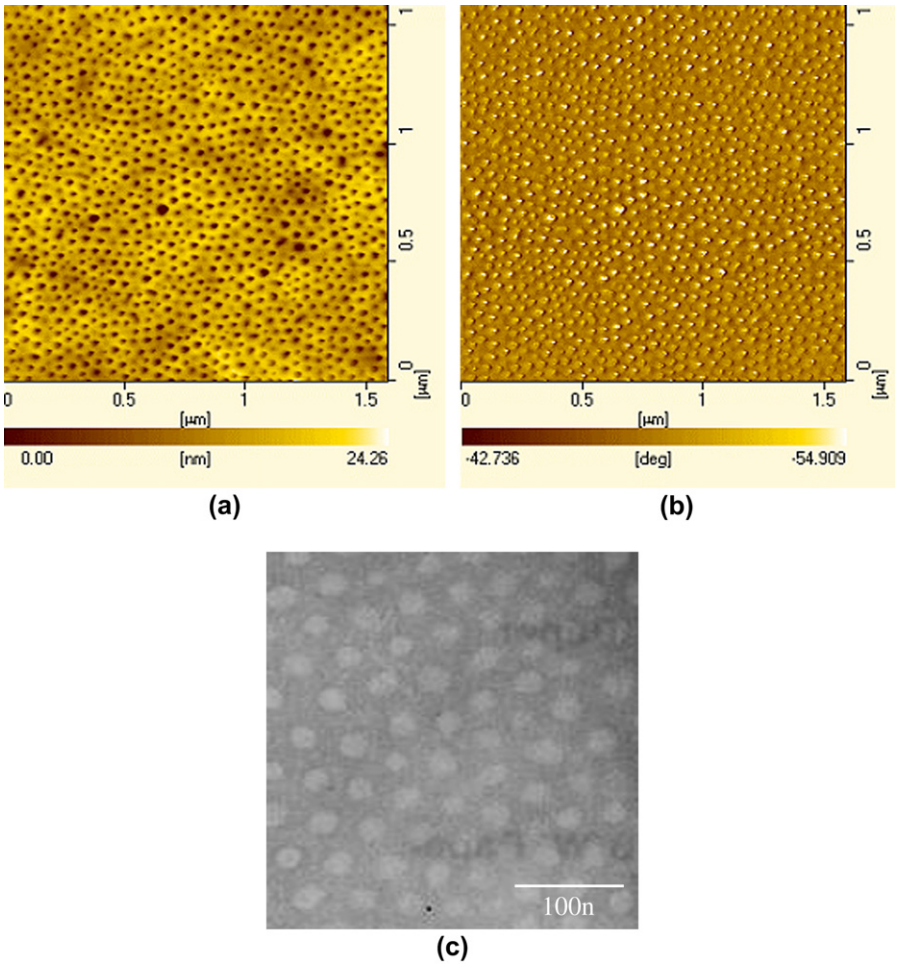

Fig. 3. AFM (a) topographic image and (b) phase image of the film cast from the solution containing PS(31 900)-*b*-P4VP(13 200)(H^+) (1.00 wt%) and PMCMA (0.29 wt%, $M_w = 7200$). (c) TEM image of the film stained with RuO_4.

this condition with a slower evaporation speed, the cylindrical nanodomains were also formed because the evaporation rate of chloroform is too fast that the polymers cannot have enough time to obtain an equilibrium state.

Fig. 3(c) shows the TEM micrograph of the film fabricated by casting the solution onto the TEM copper grid covered by carbon thin film. RuO_4 was used as the staining agent for the TEM investigation. In this case, only PS appears black in the TEM micrograph. As shown in Fig. 3(c), PS formed the continuous phase, and the hexagonal-packed nanodomains were formed by P4VP(H^+) and PMCMA. The TEM result is consistent with the AFM result. As discussed above, because the solubility of P4VP and PMCMA is larger than that of PS, the depression of the hexagonally packed nanodomains formed by P4VP(H^+) and PMCMA with respect to the PS-rich phase was formed.

The slighter interaction difference between solvent and polymers influences the phase behavior of diblock copolymer [22]. The effect of casting solvent on the formation of nanoholes was also investigated. Compared with the solubility in chloroform [$\delta_{chloroform} = 9.3\ (cal\ cm^{-3})^{1/2}$], the solubility of PS [$\delta_{PS} = 9.1\ (cal\ cm^{-3})^{1/2}$] in tetrahydrofuran [$\delta_{tetrahydrofuran} = 9.1\ (cal\ cm^{-3})^{1/2}$] is higher than that of PMCMA [$\delta_{PMCMA} = 9.3\ (cal\ cm^{-3})^{1/2}$] and P4VP [$\delta_{P4VP} = 9.2\ (cal\ cm^{-3})^{1/2}$] [59]. After spin-coating the mixture of PS-*b*-P4VP(H^+) and PMCMA from tetrahydrofuran onto the silicon substrate, PS phase should be lower than the phase of P4VP(H^+) and PMCMA. However, the featureless film with some protrusions was obtained (not shown). A possible reason is that during the process of evaporation of tetrahydrofuran, the phase separation of PMCMA from tetrahydrofuran took place first because the lower solubility compared with P4VP(H^+) and PS, and the structures of supramolecules were destroyed.

The noncovalent bond interactions are considerably weaker than the covalent bond interactions, and dependent on the external stimuli such as temperature, etc. To explore whether changing the interactions between PMCMA and P4VP(H^+) would have a remarkable effect on the nanostructures' formation, two methods were employed. One is to anneal the sample at high temperatures and the other is to increase the M_w of PMCMA and the block of P4VP. When the spin-coated film (PS(31 900)-*b*-P4VP(13 200)(H^+) (1.00 wt%) and PMCMA (0.29 wt%, $M_w = 7200$) without removing the residual solvents was annealed at 112 °C for 24 h, the residual solvent could induce the polymer chains to move and the disordered pattern was obtained because the supramolecules were

destroyed. Thus, the cylindrical nanodomains formed by P4VP(H^+) and PMCMA were destroyed, and the phase separation among the three polymers, PS, P4VP(H^+) and PMCMA occurred. The film turned to be featureless (not shown). Also, we annealed the bulk sample without residual solvents at 160 °C for 12 h to check the equilibrium morphology of bulk samples via SAXS (Fig. 4). We have not found any lamellar or perforated cylindrical microdomains. The reason may be that the supramolecules consisted of PS-*b*-P4VP(H^+) and PMCMA were broken at high temperatures because the electrostatic interactions between P4VP(H^+) and PMCMA were destroyed. The repulsive force between P4VP(H^+) and PMCMA also increased when the M_w of PMCMA increased from 7200 to 36 700. Thus, it is speculated that the electrostatic interaction is not strong enough to make the chains of PMCMA and P4VP(H^+) join together while the repulsive force is strong. Then the self-assembly behavior cannot occur when PMCMA ($M_w = 36\,700$) was employed (not shown).

As we know, the block copolymers demonstrate a variety of bulk morphologies (lamellar, double gyroid, cylindrical, spherical) depending on the ratio of block lengths and the segment–segment interaction parameter [62]. To explore the effect of the ratio of block length on the self-assembly behavior of polymeric supramolecules, PS(31 900)-*b*-P4VP(13 200) was replaced by PS(21 400)-*b*-P4VP(20 700), and other conditions were all the same. When the M_w of the block of P4VP increased from 13 200 g/mol to 20 700 g/mol, the repulsive force between P4VP(H^+) and PMCMA also increased. After spin-coating the solutions containing the two polymers from chloroform under the same conditions as used for PS(31 900)-*b*-P4VP-(13 200)(H^+) and PMCMA(7200), the featureless film morphology (the film thickness: about 255 nm) (not shown) was found since the repulsive force between the two polymers increased, and the electrostatic interaction was not strong enough to make the two polymers join together. However, when the concentration of PMCMA(7200) decreased from 0.29 wt% to 0.15 wt%, after spin-coating the solution containing PS(21 400)-*b*-P4VP (20 700)(H^+) and PMCMA(7200) onto the silicon substrate, the nanoporous film (the film thickness: about 243 nm) with some defects (Fig. 5) were obtained. The reason is that the repulsive force between P4VP(H^+)(20 700) and PMCMA(7200) may be weaker at lower concentration (0.15 wt%) than that at high concentration (0.29 wt%) [63]. If all the PMCMA chains were joined with P4VP(H^+), the weight ratio between P4VP(H^+)/PMCMA and PS is 0.56/0.44. The lamellar microdomains in the equilibrium state should be expected. In this case, some defects were observed because the polymer chains of PMCMA not bonded to P4VP(H^+) separated from the mixtures. We think that not all the PMCMA chains were attached to P4VP(H^+) by the attractive interactions. So the weight ratio between P4VP(H^+)/PMCMA and PS is less than 0.56/0.44. Another reason is that the morphology obtained by spin-coating is far from equilibrium morphology since the evaporation rate of chloroform is very fast. The polymer chains not have enough time to reach the equilibrium state. Controlled by kinetics, it might be comprehensive to obtain the cylindrical nanodomains in non-equilibrium state after spin-coating the solutions onto the silicon wafer.

Interestingly, the film morphology in Fig. 1(d) has a further evolution when exposed to carbon bisulfide, a selective solvent for PS. After annealing the film of Fig. 1(d) in a vapor of carbon bisulfide for 5 h at room temperature, the surface morphology changed from regular holes to flat and featureless film (Fig. 6(b)). Prolonged exposure to saturated carbon bisulfide vapor (62 h) led to nanoholes structure again (Fig. 6(c)). The average size of the holes is about 3 nm in depth and 32 nm in diameter. Compared with the size of holes formed in Fig. 1(d), the depth is lower and the diameter is larger (Fig. 6(a,c)). After an extended duration of treatment (93 h), the film turned to be featureless again except for small protrusions (Fig. 6(d)). In order to know whether the observed rearrangement could be amplified into macroscopically detectable changes in surface properties, static water contact angles for the polymer film subjected to different treatments were determined. The contact angle of the initial nanoporous film

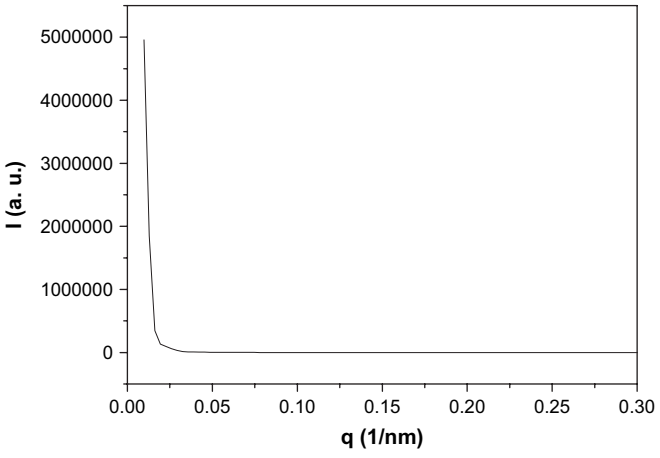

Fig. 4. SAXS intensity of PS(31 900)-*b*-P4VP(13 200)(H^+) (1.00 wt%) and PMCMA (0.29 wt%, $M_w = 7200$) annealed at 160 °C for 12 h.

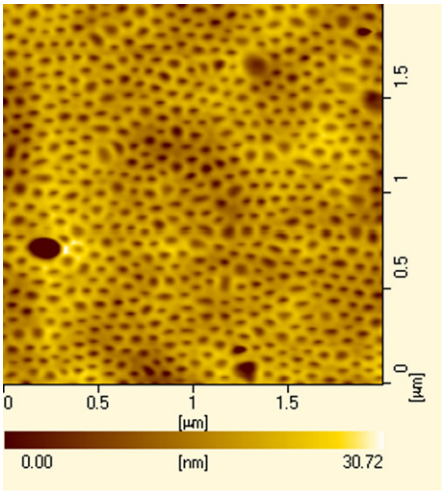

Fig. 5. AFM topographic image of the film of PS(21 400)-*b*-P4VP(20 700)-(H^+) (1.00 wt%) and PMCMA (0.15 wt%, $M_w = 7200$) spin-coated from chloroform.

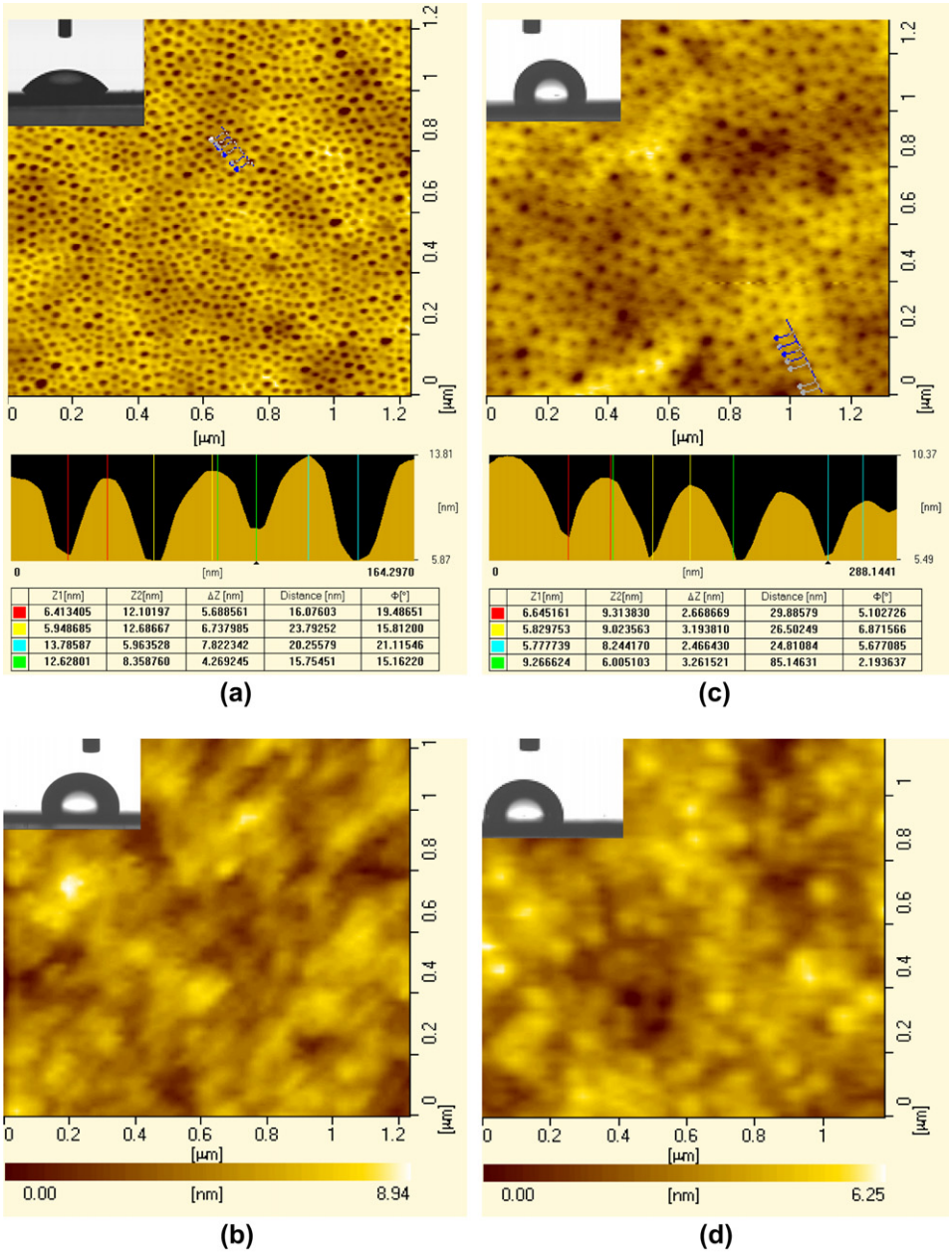

Fig. 6. AFM topographic images and the corresponding profiles of a water drop on the surfaces after the samples of Fig. 1(d) were exposed to carbon bisulfide vapor for different times: (a) 0 h; (b) 5 h; (c) 62 h; (d) 93 h.

(Fig. 6(a)) was 49°. For all the other film surfaces (Fig. 6(b–d)), the contact angles were 91°.

The XPS results show that the film surface of Fig. 6(a) is made up of three kinds of polymers: PS, P4VP(H^+) (nitrogen peak, 399.2 eV), PMCMA (C═O peak, 288.5 eV) (Fig. 7(a)). Upon exposure to carbon bisulfide, a strongly selective solvent for PS, the carbon bisulfide vapor penetrated into the PS microdomains, resulted in an increased mobility of PS. Whereas, the neighboring PMCMA and P4VP(H^+) domains were below their glass transition temperature (T_g) and still fixed. In order to increase the contact area between PS and carbon bisulfide vapor to reduce the interface energy, PS was covered on the surface of the film after 5 h carbon bisulfide vapor treatment. The contact angle of the film surface increased to 91°, a characteristic value for PS (Fig. 6(b)), indicating a hydrophobic surface. The XPS results also suggest that there are no P4VP(H^+) (nitrogen 399.2 eV) or PMCMA (C═O 288.5 eV) on the film surface (Fig. 7(b)). Therefore, the film surface properties were varied from hydrophilic to hydrophobic state because of the transformation of microscopic composition in the film surface (from PS, P4VP(H^+) and PMCMA to PS). The surface morphology of film after treated in carbon bisulfide vapor for 5 h was featureless with some protrusions. The possible reason may be that the component of PS did not reach the equilibrium state on film surface since the annealing time in carbon bisulfide vapor was short. The P4VP(H^+) and PMCMA phases might be swollen if carbon bisulfide vapor treatment time was long enough. At the moment of 62 h

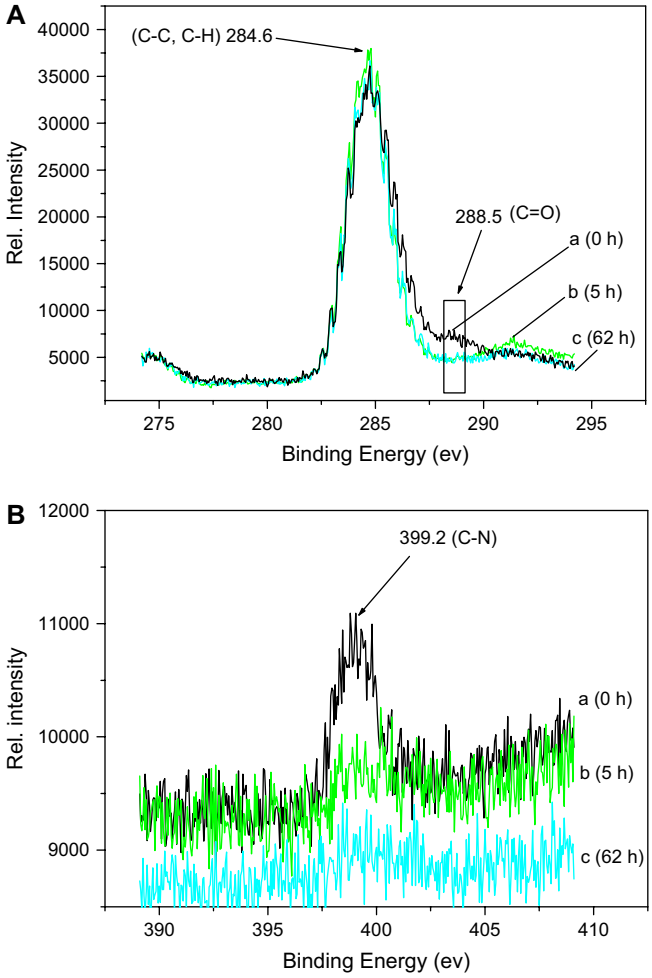

Fig. 7. XPS spectra in the (A) C1 region and (B) nitrogen region; (a) the film of Fig. 1(d) (0 h), (b) the film treated in carbon bisulfide vapor for 5 h, (c) the film treated in carbon bisulfide vapor for 62 h.

treatment in carbon bisulfide vapor, the component of PS could reach equilibrium and become a flat surface. The cylindrical nanodomains formed by P4VP(H^+) and PMCMA were covered with PS on the film surface. When the film was moved out from the environment, upon drying, the lower solubility phase (P4VP(H^+), PMCMA) solidified first, and acted as scaffold poles, while higher solubility phase (PS) was still able to shrink. The nanoporous morphology was observed after the solvent was removed. XPS results (Fig. 7(c)) also suggest that there are no nitrogen and C═O (288.5 eV) on the surface. The contact angle is still 91° (Fig. 6(c)), a characteristic value for PS. We conclude that the surface was still covered with PS, and the holes were formed due to the depression of PS-rich phase with respect to P4VP(H^+) and PMCMA-rich phases in selective solvent for PS, carbon bisulfide. It can be seen that the surface composition and wettability in Fig. 6(a,c) are different. When the annealing time was long enough (93 h), P4VP(H^+) and PMCMA were swollen by the solvent for a long time, resulted in the rearrangement of the film. Therefore, featureless film was formed. From the contact angle value (91°) (Fig. 6(d)), we concluded that the surface was also covered with PS.

4. Conclusion

The self-assembly behavior of the supramolecules consists of PS-*b*-P4VP(H^+) and a two-armed polymer with a crown ether core was investigated. Combining the electrostatic interaction and the solubility of polymers in a certain solvent, a depression of cylindrical nanodomains can be formed by the block of P4VP(H^+) and PMCMA associates surrounded by PS. Through changing the molecular weight of the polymers and annealing the film at high temperatures, we proved that proper attractive interactions between P4VP(H^+) and PMCMA played a key role in the nanostructures' formation. The effects of solvent nature and evaporation rate were also investigated. Furthermore, the surface with nanoholes can be changed to flat and featureless film upon exposure to saturated carbon bisulfide vapor at room temperature for some time. Prolonged exposure led to nanohole structure again. After an extended duration of the treatment further, the film turned to be featureless once more. However, the surface composition of the first and second nanoporous morphologies was different and the wettability changed from hydrophilic to hydrophobic state.

Acknowledgements

This work is subsidized by the National Natural Science Foundation of China (50390090, 20474065, 50573077).

References

[1] Ruokolainen J, Makinen R, Torkkeli M, Makela T, Serimaa R, Brinke G, et al. Science 1998;280:557.
[2] Tang Z, Donohoe ST, Robinson JM, Chiarelli PA, Wang HL. Polymer 2005;46:9043.
[3] Kim SH, Misner MJ, Xu T, Kimura M, Russell TP. Adv Mater 2004;16:226.
[4] Seul M, Andelman D. Science 1995;267:476.
[5] Stupp SI, LeBonheur V, Walker K, Li LS, Keser M, Amstutz A. Science 1997;276:384.
[6] Cha JN, Stucky GD, Morse DE, Deming TJ. Nature 2000;403:289.
[7] Whitesides GM, Grzybowski B. Science 2002;295:2418.
[8] Pereira RP, Rocco AM. Polymer 2005;46:12493.
[9] Wypych A, Duval E, Boiteux G, Ulanski J, David L, Mermet A. Polymer 2005;46:12523.
[10] Yang CH, Chih YK, Cheng HE, Chen CH. Polymer 2005;46:10688.
[11] Park M, Harrison C, Chaikin PM, Register RA, Adamson DH. Science 1997;276:1401.
[12] Jiang G, Wang L, Yu H, Chen C, Dong X, Chen T, et al. Polymer 2006;47:12.
[13] Chen T, Wang L, Jiang G, Wang J, Wang X, Zhou J, et al. Polymer 2005;46:7585.
[14] Kim G, Libera M. Macromolecules 1998;31:2569.
[15] Fukunaga K, Elbs H, Magerle R, Krausch G. Macromolecules 2000;33:947.
[16] Signori F, Chiellini F, Solaro R. Polymer 2005;46:9329.
[17] Efimenko K, Crowe JA, Manias E, Schwark DW, Fischer DA, Genzer J. Polymer 2005;46:9642.
[18] Jiang G, Wang L, Chen T, Yu H, Dong X, Chen C. Polymer 2005;46:9501.
[19] Knoll A, Horvat A, Lyakhova KS, Krausch G, Sevink GJA, Zvelindovsky AV, et al. Phys Rev Lett 2002;89:35501.
[20] Rehse N, Knoll A, Magerle R, Krausch G. Macromolecules 2003;36:3261.

[21] Fukunaga K, Hashimoto T, Elbs H, Krausch G. Macromolecules 2002;35:4406.
[22] Huang H, Hu Z, Chen Y, Zhang F, Gong Y, He T. Macromolecules 2004;37:6523.
[23] Matsen MW. J Chem Phys 1997;106:7781.
[24] Szamel G, Muller M. J Chem Phys 2003;118:905.
[25] Fasolka MJ, Banerjee P, Mayes AM, Pickett G, Balazs AC. Macromolecules 2000;33:5702.
[26] Wang Q, Nealey PF, de Pablo JJ. Macromolecules 2001;34:3458.
[27] Huinink HP, Brokken-Zijp JCM, van Dijk MA, Sevink GJA. J Chem Phys 2000;112:2452.
[28] Huinink HP, van Dijk MA, Brokken-Zijp JCM, Sevink GJA. Macromolecules 2001;34:5325.
[29] Huang L, He X, He T, Liang H. J Chem Phys 2003;119:12479.
[30] Horvat A, Lyakhova KS, Sevink JA, Zvelindovsky AV, Magerle R. J Chem Phys 2004;120:1117.
[31] Antonietti M, Conrad J, Thunemann A. Macromolecules 1994;27:6007.
[32] Ruokolainen J, Tanner J, Brinke G, Ikkala O, Torkkeli M. Macromolecules 1995;28:7779.
[33] Al-Hussein M, Lohmeijer BGG, Schubert US, Jeu WH. Macromolecules 2003;36:9281.
[34] Ooe M, Murata M, Mizugaki T, Ebitani K, Kaneda K. J Am Chem Soc 2004;126:1604.
[35] Gao J, Fu J, Lin C, Lin J, Han Y, Yu X, et al. Langmuir 2004;20:9775.
[36] Tang M, Dou H, Sun K. Polymer 2006;47:728.
[37] Yu X, Tang X, Pan C. Polymer 2005;46:11149.
[38] Ruokolainen J, Tanner J, Ikkala O, Brinke G, Thomas EL. Macromolecules 1998;31:3532.
[39] Manna S, Nandi AK. J Phys Chem B 2004;108:6932.
[40] van Ekenstein GA, Nijand EPH, Ikkala O, Brinke G. Macromolecules 2003;36:3684.
[41] Jiang S, Gopfent A, Abetz V. Macromolecules 2003;36:6171.
[42] Sidorenko A, Tokarev I, Stamm SMM. J Am Chem Soc 2003;125:12211.
[43] Gao L, Shi L, An Y, Zhang W, Shen X, Guo S, et al. Langmuir 2004;20:4787.
[44] Ruokolainen J, Ikkala O, Brinke G. Adv Mater 1999;11:777.
[45] Muthukumar M, Ober CK, Thomas EL. Science 1997;277:1225.
[46] Yao X, Chen D, Jiang M. Macromolecules 2004;37:4211.
[47] Ikkala O, Brinke G. Science 2002;295:2407.
[48] Wang LY, Wang ZQ, Zhang X, Shen JC, Chi LF, Fuchs H. Macromol Rapid Commun 1997;18:509.
[49] Stockton WB, Rubner MF. Macromolecules 1997;30:2717.
[50] Schubert US, Eschbaumer C. Angew Chem Int Ed 2002;41:2892.
[51] Hofmeier H, Hoogenboom R, Wouters MEL, Schubert US. J Am Chem Soc 2005;127:2913.
[52] Zhou S, Chu B. Adv Mater 2002;12:545.
[53] Akiba I, Jeong Y, Sakura K. Macromolecules 2003;36:8433.
[54] Thunemann AF. Macromolecules 2001;34:6978.
[55] Caneva D, Faul CFJ, Gotz C, Sanderson RD. Macromolecules 2003; 36:2862.
[56] Feng X, Yan L, Wen J, Pan C. Polymer 2002;43:313.
[57] Ikkala O, Ruokolainen J, Brinke G. Macromolecules 1995;28:7088.
[58] Pickett GT, Balazs AC. Macromol Theory Simul 1998;7:249.
[59] Elbs H, Fukunage K, Stadler R, Sauer G, Magerle R, Krausch G. Macromolecules 1999;32:1204.
[60] Walheim S, Boltau M, Mlynek J, Krausch G, Steiner U. Macromolecules 1997;30:4995.
[61] Zhang Q, Tsui OKC, Du B, Zhang F, Tang T, He T. Macromolecules 2000;33:9561.
[62] Bates FS, Fredrickson GH. Annu Rev Phys Chem 1990;41:525.
[63] Jeong U, Ryu DY, Kho DH, Lee DH, Kim JK, Russell TP. Macromolecules 2003;36:3626.